Journal of Alloys and Compounds 587 (2014) 474–480

Contents lists available at ScienceDirect

Journal of Alloys and Compounds

journal homepage: www.elsevier.com/locate/jalcom

Structural, electronic, phonon and thermodynamic properties of hypothetical type-VIII clathrates Ba_8Si_{46} and $Ba_8Al_{16}Si_{30}$ investigated by first principles

Payam Norouzzadeh [a], Charles W. Myles [b], Daryoosh Vashaee [a,*]

[a] Helmerich Advanced Technology Research Center, Oklahoma State University, Tulsa, OK 74106, USA
[b] Department of Physics, Texas Tech University, Lubbock, TX 79409-1051, USA

ARTICLE INFO

Article history:
Received 11 July 2013
Received in revised form 11 October 2013
Accepted 24 October 2013
Available online 1 November 2013

Keywords:
Type-VIII clathrate
Ba_8Si_{46}
$Ba_8Al_{16}Si_{30}$
Density functional theory
Lattice dynamics

ABSTRACT

We present the results of first principles calculations of the structural, electronic, elastic, vibrational, and thermodynamic properties of the hypothetical silicon-based, guest containing type-VIII clathrates Ba_8Si_{46} and $Ba_8Al_{16}Si_{30}$. We obtained the lattice constant, formation energy, band structure, density of states, elastic constants, sound velocity, and Debye temperature using the density functional theory with generalized gradient approximation (GGA). We calculated phonon dispersion and vibrational density of states spectra using the density functional perturbation energy within GGA. We computed the temperature dependent specific heat, vibrational entropy, and vibrational Helmholtz free energy by utilizing quasi-harmonic approximation. We found that replacing some silicon atoms in the framework with aluminum atoms leads to the decrease of the fundamental band gap from 1.0 in Ba_8Si_{46} to 0.18 eV in $Ba_8Al_{16}Si_{30}$. Moreover, the guest Ba atoms produced localized phonon modes lying below 1.2, 1.8 THz for Ba_8Si_{46}, and $Ba_8Al_{16}Si_{30}$, respectively, which lead to the reduction of the acoustic bandwidth of the host material. The effect of replacing Si atoms with Al on the properties of the interest is also discussed.

1. Introduction

The Group IV clathrate compounds are formed by face-shared polyhedral cages of the Group IV elements filled with alkali-metal, alkaline-earth or rare-earth atoms [1]. They connect with each other by covalent bonds. The guest-containing clathrates with only Group IV atoms on the framework, and the clathrates with some host atom substitutions are very promising from both practical and basic physics considerations. The choices of the guest atoms to vibrate inside the cage and the type and number of Group II or Group III atoms substituted on the framework may both be employed to adjust the material properties and get a broad spectrum of possible charge and thermal transport properties for them. In case of Si-based clathrates, depending on the host composition and on the guest atom choice, they show a range of various properties from wide-gap semiconductors [2] to materials with metallic conduction [3], and to superconductors [1,4] (with Na, Ba or Eu guests).

Group IV clathrates are typically promising candidates to fulfill the phonon glass electron crystal (PGEC) criteria proposed by Slack as an indicator of an efficient thermoelectric material due to their simultaneous very low lattice thermal conductivity (~1 W/m K at room temperature) and high electrical conductivity [5]. Considerable experimental and theoretical effort has been focused on finding better thermoelectric materials with PGEC properties over the past several years. The clathrates, have cages containing guest atoms which vibrate (rattle) at very low frequencies inside the cages (rattling structures). These low-lying modes resonantly scatter with the heat-carrying host acoustic phonons thus; lower the thermal conductivity [6]. Since the bonding between guest-host atoms is weak, the presence of the guest atoms usually has little effect on the host conduction bands, so that these materials have the potential to fulfill the PGEC condition.

The efficiency of energy conversion of a thermoelectric material is obtained by its dimensionless figures-of-merit $ZT = \alpha^2\sigma T/k$, where T is the absolute temperature, α is the Seebeck coefficient, σ is the electrical conductivity, and k is the thermal conductivity. It shows that an efficient thermoelectric should have good electrical conductivity and poor thermal conductivity. Therefore, we need to suppress transport of phonons and improve the charge carrier transport. The Group IV clathrate compounds have been shown to be among the good candidates for thermoelectric materials with the highest ZT [7]. These clathrates due to their relatively large lattice constants can cause short mean paths for phonon-phonon scattering and in turn cause to a reduced lattice thermal conductivity. It is notable that both the rattling atoms in the clathrate

* Corresponding author. Tel.: +1 918 594 8017.
E-mail address: daryoosh.vashaee@okstate.edu (D. Vashaee).

0925-8388/$ - see front matter © 2013 Elsevier B.V. All rights reserved.
http://dx.doi.org/10.1016/j.jallcom.2013.10.190

framework and the open nature of the framework can lead to low lattice thermal conductivity [8].

There are many available experimental and theoretical studies of the Group IV clathrates with type-I and type-II structures based on Si, Ge and Sn elements [1,9–15]. To the best of our knowledge, only six synthesized compounds in the type-VIII clathrate family (space group: I-43 m), including $Ba_8Ga_{16}Ge_{30}$ [12], $Eu_8Ga_{16}Ge_{30}$ [16], $Sr_8Ga_{16-x}Al_xGe_{30}$ ($6 < x < 10$) [17], $Ba_8Ga_{16-x}Cu_xSn_{30}$ ($0 < x < 0.033$) [18], $Sr_8Ga_{16-x}Al_xSi_{30}$ ($8 < x < 10$) [19], and $Sr_8Ga_xSi_{46x}$ [20–22] have been reported so far.

The present study was prompted by the following facts. First, the type-I clathrate $Ba_8Al_{16}Si_{30}$, which is already synthesized [23,24], has a small thermal conductivity of 4.2 W/mK [25]. The Seebeck coefficient and electrical conductivity above room temperature for this material have been also reported by Kuznetsov et al. [26]. From these values, the estimated ZT value for $Ba_8Ga_{16}Si_{30}$ was approximately 0.87 at 870 K. Also, the optimally p-type doped $Eu_8Ga_{16}Ge_{30}$-VIII clathrate was predicated to have $ZT \approx 1.2$ at 400 K [20]. These findings suggested that the silicon based clathrates may have better thermoelectric performance than the germanium based clathrates at high temperature. Second, comparing type-I and type-VIII clathrates, the p-type type-VIII clathrates are generally more favorable for their higher Seebeck coefficient and reasonable electrical conductivity. Therefore, they are expected to result in a higher ZT [1,27]. Kishimoto et al. have also shown experimentally that $Sr_8Al_xGa_{16-x}Si_{30}$ type-VIII clathrates have higher mobility than type-I (24 $cm^2\,V^{-1}\,s^{-1}$ at 300 K compared to 5 $cm^2\,V^{-1}\,s^{-1}$) [28]. Also, similar enhancement has been observed for type-VIII $Eu_8Ga_{16}Ge_{30}$ compared to type-I [19]. Bentien et al. also showed that the type-VIII clathrates $Eu_8Ga_xGe_{46-x}$ have higher mobility values than those of type-I clathrates [29]. Our purpose in this work was to find out how the change of the crystal structure (from type-I to type-VIII) would affect the basic electronic, elastic, structural, vibrational, and thermodynamic properties of these compounds. The calculated material properties provide the required parameters for further calculations of the thermoelectric transport properties with semi-classical approaches like Boltzmann Transport Equation.

We have recently calculated the electronic, vibrational, and thermodynamic properties of the pristine Si_{46}-VIII clathrate [30] and the corresponding thermoelectric transport properties [31]. The band structure of Si_{46}-VIII showed an interestingly large number of closely packed electron pockets near both the conduction and valance band edges. The resulting large density of states near the band edges is predicted to make a large thermoelectric power factor (>0.004 $W\,m^{-1}\,K^{-2}$) [30]. Therefore, we expect that the parental Si_{46}-VIII should provide a good starting material in search of Si based clathrate thermoelectric materials. It is known that the transport properties of the clathrates can be adjusted by the choice of the guest atoms or by the choice of the framework substitutions [32,33,14]. In fact, intercalation of clathrates by Ba and Na has been paid much attention in the past an can be explored for this purpose [34–37]. Such guest atoms are free to rattle in the framework due to their weak interaction with the host. These localized rattling processes resonantly scatter the acoustic phonon modes from the cage and reduce the thermal conductivity, [38] which prompts engineering of the pristine clathrates with adding guest atoms in their cage for enhancing their thermoelectric properties.

The results of first-principles calculations of the structural, electronic, phonon, elastic and thermodynamic properties of two Si-based type-VIII clathrate compounds are presented in this paper. To our knowledge, this work is the first reported first principles theoretical study of any silicon based guest containing type-VIII clathrate materials. Also to our knowledge, these type-VIII clathrate materials are so far purely hypothetical and none of them has yet been synthesized in laboratory.

All reported properties are calculated based on the density functional theory in the framework of generalized gradient approximation. Initially, we have optimized the geometry of each lattice structure. All the electronic structure, elastic constants, phonon and density of states, and thermodynamic properties calculations have been done using the optimized structures. By employing the quasi-harmonic approximation we predict some of the temperature-dependent thermodynamic properties such as specific heat, vibrational entropy and vibrational Helmholtz free energy.

2. Theoretical background

2.1. Crystal lattice structure

The guest-containing unit cell of the type-VIII clathrate contains 54 atoms and crystallizes in the BCC lattice structure. The unit cell structure has a dodecahedral cage with small empty spaces in each cage available. The ideal type-VIII clathrate structures are represented as a general chemical formula $A_8B_xC_{46-x}$ in which the A atoms are the guests residing inside the cages and B or C atoms are the host or framework atoms. The chemical formula for the better-known type-I clathrate materials is identical to that for the type-VIII materials discussed here. However, the type-I clathrates crystallize on the SC lattice structure while the type-VIII materials crystallize in the BCC structure. Although, the guest atoms in type-I clathrates are encapsulated in two kinds of frameworks, there is only one kind of polyhedral framework for the guest atoms in type-VIII clathrates [1]. In both aforementioned structures, the host atom is tightly bonded with 4 neighbor atoms by the sp^3 hybridizing orbital. All chemical formulas used in the following refer to type-VIII clathrates.

The type-VIII clathrate compounds have a non-centro-symmetric space group I-43m (No. 217). The unit cell of a typical guest- containing type-VIII clathrate has been depicted in Fig. 1(a). More specifics of crystal structure of the type-VIII clathrates may be found in the literature [1]. In $Ba_8Al_{16}Si_{30}$, Ba atoms are encapsulated in cages consisting of 23 atoms of Al or Si. The framework atoms occupy four Wyckoff sites, 2a, 12d, 8c, and 24g and the Ba guest atoms occupy the 8c Wyckoff positions. There are many possible unit cell configurations for the of the type-VIII clathrate $Ba_8Al_{16}Si_{30}$. Each possible configuration results from the placement of the Al atoms on the different framework lattice sites. For the calculations on $Ba_8Al_{16}Si_{30}$ presented here, we have adopted the configuration with no Al–Al bonds. This is similar to the lowest-energy configuration for type-VIII clathrate $Ba_8Ga_{16}Si_{30}$ found by Ross et al. [39]. In fact, we have also assumed that the zero Al–Al bonds configuration is the most energetically favorable one, which is similar to previous studies on Ba–Al–Ge and Ba–Ga–Ge compounds [40,41]. Guest–guest bonds are unlikely in these compounds because the average distance between the guests is ~5.5 Å, which is almost five times larger than the ionic radius of Ba; 1.35 Å.

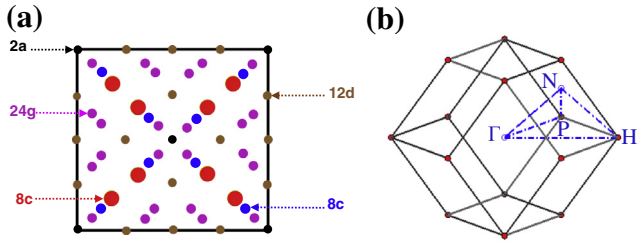

Fig. 1. (a) Crystal structure of the guest-containing type-VIII clathrate viewed along the x-direction. Guest atoms occupy 8c sites and host atoms occupy 2a, 12d, 8c, and 24g sites. (b) The first Brillouin zone of a typical type-VIII clathrate and the k-point path.

2.2. Computational methods

We used the GGA–PBE [42] exchange–correlation functional in our density functional theory (DFT) [43,44] calculations. A linear-response approach, [45–47] together with an iterative minimization, norm-conserving pseudopotential plane-wave method, as implemented in the ABINIT package has been employed [48]. The applied Troullier–Martins pseudopotentials [49–51] are single projector, and ordinary norm-conserving potentials. We used 8, 3, and 4 valence electrons for Ba, Al, and Si atoms, respectively. To ensure that the absolute total energies converged to 1 meV/atom, and that the elastic constants converged to within 2 GPa we defined a $6 \times 6 \times 6$ regular shifted k-point mesh and set the plane-wave cutoff energy to 60 Ry. We found that employing a $8 \times 8 \times 8$ grid does not change appreciably the properties of interest. The smearing method used for these calculations is the tetrahedron method. To perform the phonon property calculations we used a $8 \times 8 \times 8$ Monkhorst–Pack mesh and did not change the plane-wave energy cutoff to warrant a good coverage of the dispersion relations. The dynamical matrices were obtained from perturbation theory [46,47]. A Fourier interpolation scheme was used to increase the mesh sampling in order to improve the description of the phonon density of states (Vibrational Density of States-VDOS), the heat capacity, and the rest of properties of interest. To obtain the lattice constants, the first step in our calculations was the optimization of the lattice geometry of each compound utilizing Hellmann–Feynman forces and Broyden–Fletcher–Goldfarb–Shanno minimization procedure [52,53]. During the calculations, relaxations of both the internal structural parameters and the cell shape were included. The structural relaxation was performed until the residual forces and stresses were less than 5×10^{-5} Hartree/Bohr and 5×10^{-7} Hartree/Bohr^3, respectively. For the calculated phonon frequencies the convergence was achieved within 1 cm^{-1}. In all calculations, a supercell which is a single unit cell was employed due to relatively large unit cell of clathrates (lattice constant ~10.5 Å in average).

2.3. Elastic constants

To obtain mechanical properties of a material a full set of single-crystal elastic constants are needed. The three elastic stiffness constants C_{11}, C_{12}, and C_{44} can fully describe the elastic properties of a cubic crystal. The ABINIT code can provide these three constants C_{ij} by straining the lattice at fixed volumes [54]. The free energy was calculated then as a function of the strain. The single-crystal elastic constants of Ba_8Si_{46} and $Ba_8Al_{16}Si_{30}$ are listed in Table 1. The bulk modulus B, and tetragonal shear modulus C' can be calculated from three independent C_{ij} as:

$$B = \frac{C_{11} + 2C_{12}}{3} \tag{1}$$

and

$$C' = \frac{C_{11} - C_{12}}{2} \tag{2}$$

The shear modulus G can be obtained by the Hill modulus [55] $G_H = 1/2(G_R + G_V)$, where the G_R and G_V are determined by the following formulas [56]:

Table 1
The predicted values of lattice constants, formation energies and fundamental band gaps for the clathrates of interest are summarized in Table 1.

Type-VIII clathrate	Ba_8Si_{46}	$Ba_8Al_{16}Si_{30}$
Lattice constant (Å)	10.38	10.59
Formation energy (kJ/mol)	−94.05	−596.6
Fundamental band gap (eV)	1	0.18
Density (g/cm^3)	3.550	3.323

$$G_R^{-1} = \frac{2}{5}C'^{-1} + \frac{3}{5}C_{44}^{-1} \tag{3}$$

and

$$G_V = \frac{2}{5}C' + \frac{3}{5}C_{44}. \tag{4}$$

Young's modulus E is expressed as:

$$E = \frac{9BG}{3B + G} \tag{5}$$

Given the bulk, and shear modulus, the longitudinal v_L and the transversal v_T sound velocities were calculated using the following relations [57]:

$$\rho v_L^2 = B + \frac{4}{3}G \tag{6}$$

and

$$\rho v_T^2 = G \tag{7}$$

where ρ is the density. The average speed of sound was determined by:

$$v_s^{-3} = \frac{1}{3}\left(\frac{1}{v_L^3} + \frac{2}{v_T^3}\right) \tag{8}$$

Having the longitudinal and transversal velocities, the Debye temperature was calculated as [58]:

$$\theta_D = \frac{h v_s}{k_B}\left[\frac{3}{4\pi}\left(\frac{N_A \rho}{M}\right)\right]^{\frac{1}{3}} \tag{9}$$

where h, k_B, N_A, and M, are Planck's constant, Boltzmann's constant, Avogadro's number, and average molecular weight, respectively.

2.4. Phonon spectra and thermodynamic properties

For the calculation of the phonon spectra and temperature dependent thermodynamic properties, we have employed the ABINIT implementation where the density functional perturbation theory (DFPT) was used. First, we calculated the phonon spectra and density of states for further description of the thermal properties of the type-VIII clathrates of interest. We obtained linear response properties such as phonon frequencies as the second-derivatives of the total energy with respect to atomic displacements within the framework of the DFPT. The linear response method allowed the calculations of the dynamical matrix at any arbitrary wave vectors. Fourier transform of the dynamical matrices obtained for a grid in the first Brillouin zone (BZ) was employed to extract the force constants. We then used Fourier interpolation with specific treatment of the long-range dipole–dipole interaction to obtain the phonon spectra based on the interatomic force constants [46]. The role of spin–orbit coupling was considered for the calculation of phonon frequencies at the Γ point. By applying a tetrahedron method and a $8 \times 8 \times 8$ grid we also calculated the phonon density of states [59,60]. The thermodynamic properties of the clathrates were calculated using the quasi-harmonic approximation assuming that the system is a perfect crystalline lattice and that only the lattice vibrations contribute to the entropy. Since all phonon eigenvalues were obtained at $T = 0$ K, anharmonic effects were assumed to be negligible.

We calculated the vibrational Helmholtz free energy (F_{vib}), entropy (S_{vib}) and specific heat at constant volume (C_v) from vibrational density of states (VDOS). The procedure to obtain VDOS is outlined elsewhere [61]. In addition to the fact that we used equilibrium volumes in all our calculations, the thermal expansion coefficient is very small in semiconductors up to a few hundred degrees above room temperature. To simplify the calculations,

we calculated VDOS at 0 K and ignored temperature dependence of the lattice constant which seem reasonable because in diamond-structure Si as an example, the thermal expansion coefficient is $\sim 4.68 \times 10^{-6}\ K^{-1}$ at room temperature [62].

In the quasi-harmonic approximation, the phonon Helmholtz free energy is determined by:

$$F_{vib}(T) = k_B T \int_0^{\infty} \left[\frac{1}{2}\hbar\omega + k_B T \ln\left(1 - e^{-\frac{\hbar\omega}{k_B T}}\right)\right] g(\omega) d\omega \quad (12)$$

where k_B is the Boltzmann constant. The VDOS is normalized such that $\int g(\omega)d\omega = 3N$, where N is the number of atoms. The zero point phonon energy is defined by F_{vib} at $T = 0$ K. The phonon entropy and the specific heat at constant volume are respectively given by:

$$S_{vib}(T) = \left(\frac{\partial F_{vib}}{\partial T}\right)_V \quad (13)$$

and

$$C_V(T) = -T\left(\frac{\partial^2 F_{vib}}{\partial T^2}\right)_V \quad (14)$$

3. Results and discussion

Following the structural optimization and through calculation of GGA minimum total energies as functions of volume and then by fitting the Energy–Volume data to the third order Birch–Murnaghan equation of state [63], we obtained lattice constants of 10.38, and 10.59 Å for Ba_8Si_{46} and $Ba_8Al_{16}Si_{30}$ clathrates, respectively. The predicted lattice constants indicate that the substitution of the 16 Si atoms by Al atoms expands the framework. This is understandable by comparing the larger atomic radius of Al with the smaller atomic radius of Si. Fig. 2 depicts our calculated electronic band structures and densities of states for the two clathrates of interest. Fig. 2(a) and (b) indicate that the band structures are complex, the number of bands is very large due to the large number of atoms in a unit cell.

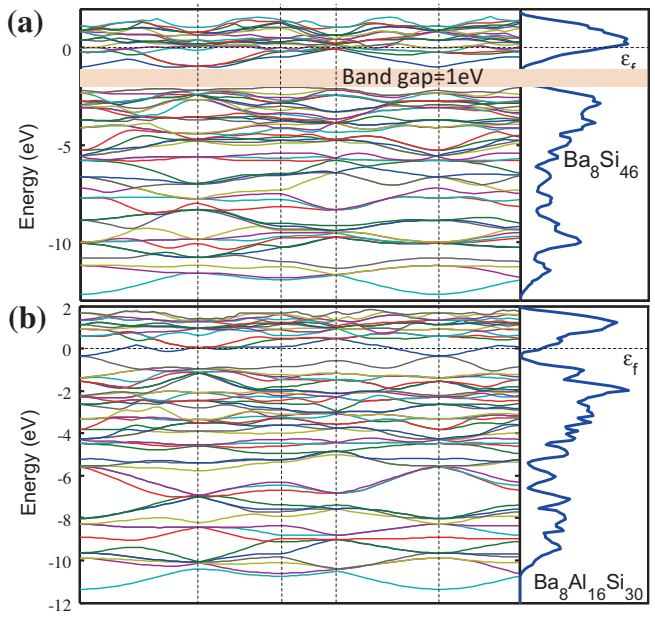

Fig. 2. GGA electronic band structures and scaled total density of states for (a) Ba_8Si_{46} and (b) $Ba_8Al_{16}Si_{30}$. Each figure displays the energy bands along several symmetry directions of the first Brillouin zone. In units of $2\pi/a$, the labeled k points correspond to $\Gamma = (0,0,0)$, $H = (1/2,1/2,-1/2)$, $N = (1/2,0,0)$ and $P = (1/4,1/4,1/4)$. The Fermi level is set to 0 eV and is shown by horizontal dashed line. The dark salmon colored rectangles show the band gaps.

Flatness of the bands makes the determination of the k-point to k-point transition for the minimum energy gap, especially near the Fermi level at the top of the valence band difficult in these clathrates. Our calculations show that the Ba_8Si_{46}-VIII should has a band gap between the Brillouin zone points $N = (1/2,0,0)$ and a k point between Gamma = $(0,0,0)$ and $H = (1/2,1/2,-1/2)$ points. We predict that the $Ba_8Al_{16}Si_{30}$-VIII compound has a much smaller fundamental band gap. The valence electrons from Ba and Al atoms contribute in conduction band and due to increment of screening effects, result in narrowing the fundamental band gap in these metal doped compounds. The valence and conduction bands almost touch each other at the Gamma point in $Ba_8Al_{16}Si_{30}$-VIII compound. The predicted fundamental GGA band gaps of the Ba_8Si_{46} and $Ba_8Al_{16}Si_{30}$ clathrates are approximately 1.0 and 0.18 eV, respectively. These values of band gaps show that replacing 16 Si atoms with Al atoms on the framework causes a significant reduction in the band gap, which can be attributed to the unpaired electron in the p-orbital of Al. The p-orbitals of Si atoms hybridize with those of the Al atoms, which in turn reduces the band gap of $Ba_8Al_{16}Si_{30}$. It is also notable that, Ba guest atoms donate their electrons to the anti-bonding states (conduction bands) of the host material. The differences in the hybridized states of the framework originate from the wave function overlap between the guest and host atoms.

Our calculated results for the total scaled electronic density of states (DOS) for each compound of interest are presented in Fig. 2(a) and (b). The calculated densities of states are qualitatively similar to each other. The Fermi level of Ba_8Si_{46} is located closely to the peak in conduction band which can be attributed to strong hybridization between Ba states and Si_{46} conduction band. In contrast, in $Ba_8Al_{16}Si_{30}$-VIII compound the location of Fermi level is away from the peak in conduction band. Each scaled total electronic density of states has two major regions, an s region and a p bonding region. The electronic states of the valence electrons are formed by sp^3 orbitals so the main contribution to these states comes from p orbitals.

We also calculated the formation energies E_f for the Ba_8Si_{46} and $Ba_8Al_{16}Si_{30}$ clathrates. Energy of formation refers to the electronic part of the formation energy with respect to the elements in their standard state. The energies of formation were calculated from the following relation:

$$E_f(Ba_8Al_{16}Si_{30}) = E_{Ba_8Al_{16}Si_{30}} - 8E_{Ba} - 16E_{Al} - 30E_{Si} \quad (15)$$

in which EBa is the energy per Ba atom in Ba metal, and similarly for all other atoms. Similar formula was also applied to Ba8Si46 material. The formation energy determines if it is energetically favorable for a material to form in comparison with the solids formed by its constituents (Ba, Al, and Si). We find that the formation energies for Ba_8Si_{46} and $Ba_8Al_{16}Si_{30}$ are −94.05 and −569.60 kJ/mol per unit cell, respectively. These results predict that the guest containing clathrates Ba_8Si_{46} and $Ba_8Al_{16}Si_{30}$ are thermodynamically more stable than their isolated bulk constituents; hence, it is energetically favorable for them to form.

3.1. Elastic properties

The mechanical properties for the aforementioned clathrates were calculated at their theoretical equilibrium volumes. We set the strain values to 0.005. The eigenvalues of the elastic stiffness matrix were found to be (13.72, 327.23, 13.72, 3.66, 3.66, 3.66), and (80.14, 203.76, 80.14, 184.89, 184.89, 184.89) for Ba_8Si_{46} and $Ba_8Al_{16}Si_{30}$ respectively, indicating that the matrices are positive-definite, and that the clathrate crystals are mechanically stable. The calculated values of the elastic constants, bulk, shear, and Young's moduli, longitudinal, transverse, and mean sound veloci-

Table 2
Calculated elastic constants C_{ij}, bulk B, shear G, and Young's E moduli in GPa, longitudinal, transverse, and mean sound velocities in m/s, and Debye temperatures in K for Ba_8Si_{46}, and $Ba_8Al_{16}Si_{30}$.

Type-VIII clathrate	Ba_8Si_{46}	$Ba_8Al_{16}Si_{30}$
C_{11} (GPa)	125.46	121.32
C_{12} (GPa)	43.26	41.23
C_{44} (GPa)	46.5	46.20
B (GPa)	76.66	67.93
G (GPa)	45.17	43.63
E (GPa)	109.57	107.80
v_L (m/s)	6777	6160
v_T (m/s)	4080	3623
v_S (m/s)	4509	4016
θ_D (K)	468	427

ties along with Debye temperature for each compound have been listed In Table 2.

As can be seen from Table 2, the predicted values of all listed elastic properties are reduced by replacing Si atoms by Al atoms in the framework.

3.2. Phonon spectra and VDOS

In theory of lattice dynamics, the collective motion of all atoms in lattice is described by vibrational eigenvalues or phonon spectra. Fig. 3(a) and (b) present our calculated ground state phonon dispersion curves at $T = 0$ K respectively for the type-VIII clathrates Ba_8Si_{46} and $Ba_8Al_{16}Si_{30}$ along with their corresponding phonon density of states (VDOS).

The phonon spectra for the two materials are very similar and share relatively common features. The acoustic modes are located below approximately 2, and 3 THz for the Ba_8Si_{46}, and $Ba_8Al_{16}Si_{30}$ materials, respectively, and the optical modes lie above that range. There are two high densities of states regions in each material. One region is above the acoustic modes in the ranges of 2–4.5 and 3–5.8 THz for Ba_8Si_{46}, and $Ba_8Al_{16}Si_{30}$, respectively, and the other region is near the top of the optical branch above 9, and 8.8 THz, accordingly. We expect that the contribution of optical modes to heat transport will be small [64]. The highest optical modes are located at 11.4 and 12.2 THz for Ba_8Si_{46}, and $Ba_8Al_{16}Si_{30}$, respectively.

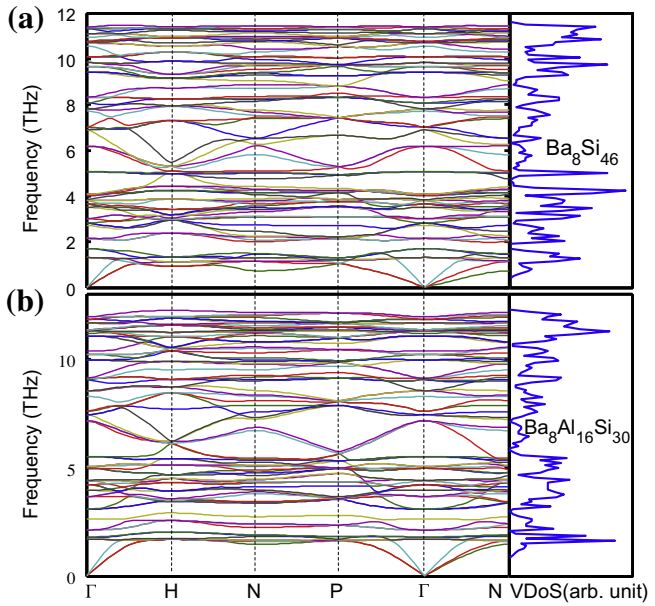

Fig. 3. Calculated phonon dispersion relations and vibrational density of states for (a) Ba_8Si_{46} and (b) $Ba_8Al_{16}Si_{30}$.

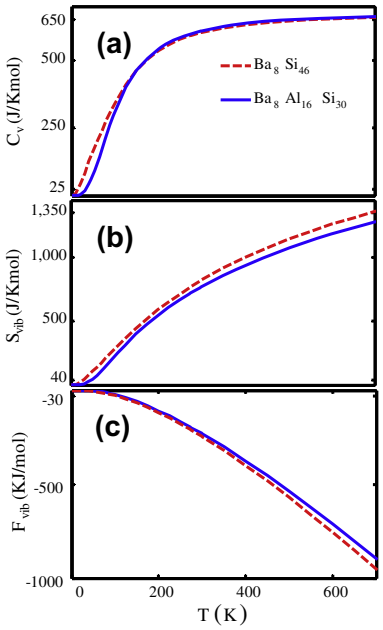

Fig. 4. Calculated thermodynamic properties of Ba_8Si_{46} (red curves), and $Ba_8Al_{16}Si_{30}$ (blue curves) in the temperature range 0–700 K. (a) Specific heat at constant volume C_v, (b) vibrational entropy S_{vib}, and (c) vibrational Helmholtz free energy F_{vib}. (For interpretation of the references to color in this figure legend, the reader is referred to the web version of this article.)

The calculated VDOS for both materials increases above both regions of acoustic and optic branches. The top of the acoustic bands are located at about 1.2 and 1.8 THz, respectively, for Ba_8Si_{46}, and $Ba_8Al_{16}Si_{30}$. It means that, in comparison to that of $Ba_8Al_{16}Si_{30}$, the acoustic bandwidth in Ba_8Si_{46} clathrate is reduced by about 67%. These results also show that replacing Si atoms by Al atoms in the framework leads to a wider bandwidth for the heat-carrying acoustic modes. In fact, suppression of the acoustic bandwidth becomes less effective after replacing Si atoms by Al atoms.

The weak bonding of the guest atoms in the framework as a consequence of avoided crossing effect results in low frequency localized guest atom phonon modes which, in heat transport theory, can couple to the lattice modes by resonantly scattering the heat-carrying acoustic modes of the host [65]. This should increase the probability of resonant scattering of the host acoustic phonons, and thus should lead to a lower lattice thermal conductivity. The phonon modes near the transition region of the acoustic- to optic-mode range allow thermal energy transfer from the framework to the guest atoms due to their dual nature [61]. As can be seen in Fig. 3, we also find gaps in both the phonon dispersion curves and the VDOS within the optic bands. These gaps are located in the ranges 1.75–2.05 THz for Ba_8Si_{46}, and 2.03–2.12, 2.55–2.6 and 2.91–3.08 THz for $Ba_8Al_{16}Si_{30}$. The existence of these gaps is not usual in covalently bonded compounds. These gaps are unique feature of clathrates which possibly are caused by the open structure and interconnected cages of their lattices [66]. It is notable that, in molecular solids, the high energy intramolecular modes (caused by the cage atoms) are separated from the low energy intermolecular modes (guest-cage modes), which results in these gaps.

3.3. Thermodynamic properties

We have also calculated the phonon contributions to the specific-heat capacity at constant volume, the entropy, and the Helm-

holtz free energy in the Ba_8Si_{46}, and $Ba_8Al_{16}Si_{30}$ type-VIII clathrate materials in the temperature range 0–700 K. In the theory of the lattice dynamics, the specific heat at constant volume is more easily calculated than the specific heat at constant pressure, which is the more common experimentally measurable quantity. For solids, the two specific heats are related by $C_p - C_v = BTV\alpha_V^2$, where α_V is the volumetric coefficient of thermal expansion, B is the bulk modulus, T is the absolute temperature, and V is the volume. Our calculated temperature-dependent specific heat, vibrational entropy, and the vibrational Helmholtz free energy for Ba_8Si_{46}, and $Ba_8Al_{16}Si_{30}$ have been demonstrated in Fig. 4(a) and (b) respectively. The temperature dependencies of all quantities of interest show similar features for the two materials. In Fig. 4(a) the C_v curves increase smoothly with temperature in the range 0–700 K. At approximately 300 K, C_v begins to approach the Dulong and Petit value of $3NR$, where R is the gas constant and N is the number of atoms in the unit cell. As the temperature increases above about 300 K the C_v curves become almost flat. This indicates that the optical and acoustic modes of these clathrates are all excited at room temperature. As can be seen from Fig. 4(a), we predict that the substitution of Si atoms by Al atoms in the framework will have a negligible effect on the vibrational heat capacity. Our calculations predict that at $T = 300$ K, C_v for Ba_8Si_{46}, and $Ba_8Al_{16}Si_{30}$ is 604.15, and 626.17 J/K mol, correspondingly.

Fig. 4(b) shows the calculated temperature-dependent vibrational entropies for Ba_8Si_{46}, and $Ba_8Al_{16}Si_{30}$. The calculated vibrational entropies at $T = 300$ K are 820.77 and 859.28 J/K mol, respectively for the clathrates of interest. As the temperature increases the entropy curves increase smoothly as well. This behavior is understandable because the phonon frequencies should increase with temperature.

The vibrational Helmholtz free energies as a function of temperature for the Ba_8Si_{46}, and $Ba_8Al_{16}Si_{30}$ materials have been plotted in Fig. 4(c). It is known that the free energy of a compound is a function of its geometrical structure. From Fig. 4(c), it can be seen that the substitution of Si atoms by Al atoms in the framework leads to more stable clathrate compounds.

4. Conclusions

We calculated the structural, electronic, elastic, phonon and thermodynamic properties of two hypothetical type-VIII clathrates Ba_8Si_{46}, and $Ba_8Al_{16}Si_{30}$ from the first principles methods. Several properties of these clathrates and the results of these calculations were presented using GGA DFT computational scheme. Primarily, we started from the pristine type-VIII clathrate Si_{46} and added Ba guest atoms to the cage to form Ba_8Si_{46}. Later, we then constructed the unit cell of $Ba_8Al_{16}Si_{30}$ by selecting a configuration with zero Al–Al bonds. The geometries of each of the two clathrates were then optimized. Our calculations predict that the fundamental band gap of $Ba_8Al_{16}Si_{30}$-VIII is much smaller than that of Ba_8Si_{46}-VIII. The predicted band gaps are about 1.0 and 0.18 eV, respectively, for Ba_8Si_{46}, and $Ba_8Al_{16}Si_{30}$. In addition, the effect on the lattice constant and on the formation energy of the substitution of Al on the framework was investigated. The predicted elastic constants show clear trends as a result of the substitution of some of the Si atoms by Al. We also showed that replacing Si atoms by Al atoms increased the acoustic bandwidth which leads to an increment of lattice thermal conductivity. Finally, we have calculated the temperature-dependent vibrational specific heat, entropy, and the Helmholtz free energy for the clathrates of interest. Our calculations show that the temperature variations of these properties demonstrate similar features as those found for other clathrate compounds [67–69].

Acknowledgements

This work was partially supported by AFOSR under Grant No. FA9550-10-1-0010 and the National Science Foundation (NSF) under Grant No. 0933763. The authors would like to thank the Texas Tech and Oklahoma State Universities High Performance Computing Centers for many hours of computing time.

References

[1] S. Paschen, W. Carrillo-Cabrera, A. Bentien, V.H. Tran, M. Baenitz, Y. Grin, F. Steglich, Phys. Rev. B 64 (2001) 214404.
[2] M. Menon, E. Richter, K.R. Subbaswamy, Phys. Rev. B 56 (2002) 12290.
[3] D. Connétable, Phys. Rev. B 75 (2007) 125202.
[4] R.F.W. Herrmann, K. Tanigaki, S. Kuroshima, H. Suematsu, Chem. Phys. Lett. 283 (1) (1998) 29–32. 4.
[5] G.A. Slack, in: D.M. Rowe (Ed.), CRC Handbook of Thermoelectrics, CRC, Boca Raton, 1995, p. 407.
[6] C.W. Myles, J. Dong, Otto F. Sankey, Phys. Status Solidi (b) 239 (1) (2003) 26–34.
[7] G.J. Snyder, E.S. Toberer, Nat. Mater. 7 (2008) 105–114.
[8] G.S. Nolas, M. Beekman, J. Gryco, G.A. Lamberton Jr., T.M. Tritt, P.F. McMillan, Appl. Phys. Lett. 82 (2003) 910.
[9] H. Fukuoka, J. Kiyoto, S. Yamanaka, Inorg. Chem. 42 (2003) 2933.
[10] M. Imai, K. Nishida, T. Kimura, K. Yamada, J. Alloys Comp. 335 (2002) 270.
[11] J. Dong, O.F. Sankey, J. Phys.: Condens. Matter 11 (1999) 6129.
[12] G.S. Nolas, J.L. Cohn, J.S. Dyck, C. Uher, J. Yang, Phys. Rev. B 65 (2002) 165201.
[13] G.S. Nolas, D.G. Vanderveer, A.P. Wilkinson, J.L. Cohn, J. Appl. Phys. 91 (2002) 8970.
[14] K. Biswas, C.W. Myles, Phys. Rev. B 75 (2007) 245205.
[15] K. Biswas, C.W. Myles, Phys. Rev. B 74 (2006) 115113.
[16] B.C. Sales, B.C. Chakoumakos, R. Jin, J.R. Thompson, D. Mandrus, Phys. Rev. B 63 (2001) 245113.
[17] Y. Sasaki, K. Kishimoto, T. Koyanagi, H. Asada, K. Akai, J. Appl. Phys. 105 (2009) 073702.
[18] S. Deng, Y. Saiga, K. Kajisa, T. Takabatake, J. Appl. Phys. 109 (2011) 103704.
[19] K. Kishimoto, N. Ikeda, K. Akai, T. Koyanagi, Appl. Phys. Express 1 (2008) 031201.
[20] W. Carrllo-Cabrera, R. Cardoso Gil, Yu. Grin, Z. Kristallogr. New. Cryst. Struct. 217 (2002) 179.
[21] M. Imai, K. Nishida, T. Kmura, K. Yamada, J. Alloys Comp. 335 (2002) 270.
[22] K. Suekuni, M.A. Avila, K. Umeo, T. Takabatake, Phys. Rev. B. 75 (2007) 195210.
[23] N. Mugita, Y. Nakakohara, T. Motooka, R. Teranishi, S. Munetoh, IOP Conf. Series: Materials Science and Engineering 18 (2011) 142007.
[24] Y. Nakakohara, N. Mugita, Y. Nagatomo, M. Saisho, T. Motooka, R. Teranishi, S. Munetoh, MRS Proceedings, Vol. 1325, 2011.
[25] Jung-I1 Lee, Young-Ho Kim, Seung-Hwan Park, Soon-Chul Ur, I1-Ho Kim, in: 26th International Conference on Thermoelectrics, 2007. ICT 2007.
[26] V.L. Kuznetsov, L.A. Kunnetsova, A.E. Kaliazin, D.M. Rowe, J. Appl. Phys. 87 (2000) 7871.
[27] G.K.H. Madsen, K. Schwarz, P. Blaha, D.J. Singh, Phys. Rev. B 68 (2003) 125212.
[28] K. Kishimoto, N. Ikeda, K. Akai, T. koyanagi, Appl. Phys. Express 1 (2008) 031201.
[29] A. Bentien, V. Pacheco, S. Paschen, Yu. Grin, F. Steglich, Phys. Rev. B 71 (2005) 165206.
[30] P. Norouzzadeh, C.W. Myles, D. Vashaee, Prediction of a large number of electron pockets near the band edges in type-VIII clathrate Si_{46} and its physical properties from first principles, Journal of Physics: Condensed Matter, in press.
[31] P. Norouzzadeh, C.W. Myles, D. Vashaee, Predicting the transport properties of Si46-VIII from first principles results, in preparation.
[32] G.S. Nolas, J.M. Ward, J. Gryko, L. Qiu, M.A. White, Phys. Rev. B 64 (2001) 153201.
[33] J.L. Cohn, G.S. Nolas, V. Fessatidis, T.H. Metcalf, G.A. Slack, Phys. Rev. Lett. 82 (1999) 779.
[34] S. Saito, A. Oshiyama, Phys. Rev. B 51 (1995) 2628.
[35] V.I. Smelyanski, J.S. Tse, Chem. Phys. Lett. 264 (1997) 459.
[36] P. Mélinon et al., Phys. Rev. B 58 (12) (1998) 590.
[37] K. Moriguchi, S. Munetoh, A. Shintani, Phys. Rev. B 62 (2000) 7138; K. Moriguchi, M. Yonemura, A. Shintani, S. Yamanaka, Phys. Rev. B 61 (2000) 9859.
[38] J. Dong, O.F. Sankey, G.K. Ramachandran, P.F. McMillan, J. Appl. Phys. 87 (2000) 7726.
[39] Sergio Y. Rodriguez, Xiang Zheng, Laziz Saribaev, Joseph H. Ross Jr., Proc. Mater. Res. Soc. 1267 (2010) DD04–DD07.
[40] N.P. Blake, D. Bryan, S. Latturner, L. Mollnitz, G.D. Stucky, H. Metiu, J. Chem. Phys. 114 (2001) 10063.
[41] W. Gou, S.Y. Rorigues, Y. Li, J.H. Ross Jr., Phys. Rev. B 80 (2009) 144108.
[42] J.P. Perdew, K. Burke, M. Ernzerhof, Phys. Rev. Lett. 77 (1996) 3865.
[43] P. Hohenberg, W. Kohn, Phys. Rev. 136 (1964) B864.
[44] W. Kohn, L.J. Sham, Phys. Rev. 140 (1965) A1133.
[45] S. Baroni, P. Giannozzi, A. Testa, Phys. Rev. Lett. 58 (1987) 1861.
[46] X. Gonze, Phys. Rev. B 55 (1997) 10337.

[47] X. Gonze, C. Lee, Phys. Rev. B 55 (1997) 10355.
[48] X. Gonze, J.M. Beuken, R. Caracas, F. Detraux, M. Fuchs, G.M. Rignanese, L. Sindic, M. Verstraete, G. Zerah, F. Jollet, Comput. Mater. Sci. 25 (2002) 478. ABINIT is a common project of the Universite Catholique de Louvain, Corning Incorporated, and other contributors <http://www.pcpm.ucl.ac.be/ABINIT>..
[49] D.R. Hamann, M. Schluter, C. Chiang, Phys. Rev. Lett. 43 (1979) 1494.
[50] N. Troullier, José Luís Martins, Phys. Rev. B 43 (1991) 1993.
[51] M.C. Payne, M.P. Teter, D.C. Allan, T.A. Arias, J.D. Joannopoulos, Rev. Mod. Phys. 64 (1992) 1045.
[52] W.H. Press, S.A. Teukolsky, W.T. Vetterling, B.P. Flannery, Numerical Recipes in Fortran 77: The Art of Scientific Computing, second ed., Cambridge University Press, Cambridge, 1992. p418.
[53] C.G. Broyden, J. Inst. Math. Appl. 6 (1970) 76;
R. Fletcher, Comput. J. 13 (1970) 317;
D. Goldfarb, Math. Comput. 24 (1970) 23;
D.F. Shanno, Math. Comput. 24 (1970) 647.
[54] D.R. Hamann, X. Wu, K.M. Rabe, D. Vanderbilt, Phys. Rev. B 71 (2005) 035117.
[55] R. Hill, Proc. Phys. Soc. London 65 (1952) 349.
[56] L. Vitos, Computational Quantum Mechanicals for Materials Engineers, Springer-Verlag, London, 2007.
[57] H.M. Ledbetter, J. Appl. Phys. 44 (1973) 1451.
[58] G. Grimvall, Thermophysical Properties of Materials, North-Holland, Amsterdam, 1999.
[59] O. Jepson, O.K. Andersen, Solid State Commun. 9 (1971) 1763.
[60] G. Lehmann, M. Taut, Phys. Status Solidi B 54 (1972) 469.
[61] J.J. Dong, O.F. Sankey, G.K. Ramachandran, P.F. McMillan, J. Appl. Phys. 87 (2000) 7726.
[62] R. Hull, Properties of Crystalline Silicon, INSPEC, London, 1999.
[63] The Birch–Murnaghan equation for the energy E as a function of volume V is $E(V) = E_0+9/8(KV_0)[(V_0/V)2/3-1]2\{1+[(4-K')/2][1-(V_0/V)^{2/3}]\}$. E, E_0, V, V_0, K and K' are the energy, minimum energy, the volume, volume at the minimum energy, the bulk modulus and its pressure derivative respectively.
[64] N.W. Ashcroft, N.D. Mermin, Solid State Physics, Holt, Reinhart, and Winston, New York, 1976.
[65] G.S. Nolas, G.A. Slack, S.B. Schujman, in: T.M. Tritt (Ed.), Recent Trends in Thermoelectric Materials Research I, Semiconductors and Semimetals, vol. 69, Academic, San Diego, 2000 (references therein).
[66] D. Kahn, J.P. Lu, Phys. Rev. B 56 (1997) 13898.
[67] A. Bentien, S. Johnsen, Bo B. Iversen, Phys. Rev. B 73 (2006) 094301.
[68] L. Qiu, I.P. Swainson, G.S. Nolas, M.A. White, Phys. Rev. B 70 (2004) 035208.
[69] L. Qiu, M.A. White, Z. Li, J.S. Tse, C.I. Ratcliffe, C.A. Tulk, J. Dong, O.F. Sankey, Phys. Rev. B 64 (2001) 024303.